Proceedings of the ASME 2024
International Design Engineering Technical Conferences and
Computers and Information in Engineering
IDETC-CIE 2024
August 25-28, 2024, Washington, DC, USA

IMECE2024-####

DESIGN AND MODELING OF COMPLIANT FOUR-BAR MECHANISMS WITH VARIABLE STIFFNESS LINKS FOR MULTI-OUTPUT TRAJECTORY

Jiayu Luo², Muhammad Hammad Alvi², Han Lin², Xiaotong Huang², Dongming Gan¹

¹Purdue University, West Lafayette, IN, USA, *corresponding: <u>dgan@purdue.edu</u>
²Purdue University, West Lafayette, IN, USA

ABSTRACT

This research presents a novel design of a four-bar mechanism featuring a variable stiffness link (VSL) as the output component, aimed at enabling diverse end-effector trajectories without modifying the link length or moment input. By employing both single-beam and multi-section beam configurations within a large deflection model, the study investigates the effect of varying link stiffness under constant load and geometric conditions on the mechanism's trajectory outcomes. The proposed design was validated through both numerical modeling and experimental testing of a built prototype. The findings confirm the prototype's alignment with theoretical predictions, highlighting the VSL's key role in significantly enhancing the adaptability and application range of four-bar mechanisms. This advancement circumvents the traditional constraints of fixedtrajectory mechanisms, proposing a versatile, efficient, and costeffective solution for complex motion applications in compliant mechanism design.

Keywords: Four-bar mechanism, variable stiffness, large deflection model

1. INTRODUCTION

The four-bar mechanism is a simple and widely used structure for force [1], moment, and energy transmission. The advantages of the four-bar mechanism include simple design and ease of construction, versatile motion control from its closed-loop nature, efficient power transmission, and highly customizable motion paths [2]. However, the traditional four-bar mechanism has a very limited trajectory for one given configuration without changing its structure such as link length or link geometry. The end-effector trajectory on a rigid four-bar mechanism is usually a single fixed curve, limiting the application range and reconfigurability of such a structure [3].

Incorporating variable stiffness link (VSL) into four-bar mechanisms can bring new aspects into the field, enabling a dynamic adjustment of the mechanism's behavior in response to varying demands [4]. This paper presents a novel design of a four-bar mechanism featuring a VSL as the output link, capable of achieving multiple end-effector trajectories without altering the link length or moment input. Through numerical modeling and experimental validation [5], encompassing both single-beam and multi-section beam configurations within a large deflection framework, the study investigates the trajectory variations under consistent load and geometric conditions.

The development of VSLs and sophisticated analytical tools for modeling non-linear compliance has led to a paradigm shift in the design and application of four-bar mechanisms [6]. By bridging the gap between traditional mechanical linkages and the need for versatile, responsive systems, this research highlights the potential of VSL-equipped four-bar mechanisms in actuation and transmission mechanical systems across various industries. The integration of flexible segments that can undergo elastic deformation, replacing the rigid joints in traditional four-bar mechanisms, introduces an enhanced level of adaptability and operational flexibility [7]. This paper underscores the practical applicability of VSLs in expanding the functional capabilities of four-bar mechanisms and explores the design implementation of compliant mechanisms.

The advent of compliant mechanisms, characterized by flexible links capable of significant deformation under load, presents a solution to this limitation by simplifying structures, reducing costs, providing self-position restoration without additional actuators, and minimizing wear, lubrication, and friction [8]. Despite their advantages, the non-linear deflection inherent in compliant mechanisms poses a substantial challenge for modeling [9]. The nonlinearity of the deflection in the compliant mechanism was a major difficulty for modeling, but multiple analytical methods have been developed, such as the large deflection model (LDM) [10], multiple section pseudo rigid body model (mPRBM) [11], beam constraint model (BCM) [12], and traditional finite element analysis (FEA). The PRBM is one of the most accurate and relatively computationally

efficient models for compliant beam deflection analysis, providing much insight into the simplification of the nonlinear behavior of compliant structures.

However, the PRBM also had some inherent drawbacks. It relied on multiple fundamental assumptions, such as using torsional springs to model flexible segments, which may not always align with the actual material behavior, and uniform force and moment conduction along the beam. Additionally, the model had limitations in handling certain deformation types like shear deformations or complex material properties [11]. Despite these limitations, the large deflection model's ability to accurately analyze compliant mechanisms undergoing large, non-linear deflections still provides valuable information for designing and modeling compliant mechanisms.

The PRBM was an important development in the field of compliant mechanism analysis in the early 1990s proposed by Howell and Mavroidis [13]. It addressed a major limitation in analyzing compliant mechanisms that undergo significant, nonlinear deformations. Traditional linear models like Euler's beam theory and finite element analysis became inaccurate and timeconsuming for these large deflections. The PRBM introduced a simplified yet accurate way to model and predict the behavior of compliant mechanisms under such conditions. The key innovation of the PRBM was representing the compliant mechanism as a system of rigid links connected by torsional spring joints. This simplified model could effectively capture the non-linear deformations and stress distributions that occur during large deflections. The PRBM offered numerous advantages, including improved accuracy over linear models [14], a straightforward approach for understanding complex mechanisms, efficient design optimization capabilities, and support for rapid prototyping by reliably predicting mechanism behavior before fabrication.

This paper introduces a novel design of a four-bar mechanism featuring a variable stiffness link (VSL) as the output component, aimed at enabling diverse end-effector trajectories without modifying the link length or moment input. We will describe the design concept in section 2, with the mathematical modeling in sections 2.1 and 2.2, and the device design and fabrication considerations in section 2.3. The results of the verification and testing are discussed in section 3 with the comparison of experimental data and modeling.

2. DESIGN AND METHODS

The four-bar mechanism is designed to have three rigid links: input link, transmission link, and ground link. The output link is compliant and has a rigid connection to the ground. All interlink joints besides the connection between the compliant link and ground link are revolute joints, allowing only motion and force transmission but not moment. A computation model with a large deflection model is completed in MATLAB to simulate the behavior of the four-bar mechanism with a compliant link, as shown in Figure 1. A physical model is fabricated with 3D-printed parts to test the structure design. The parts are designed with certain specifications and the young's module of the used material is tested and obtained by Fu's team

[15] for MATLAB model simulation. The same design is tested in finite element analysis (FEA) in ANSYS for verification.

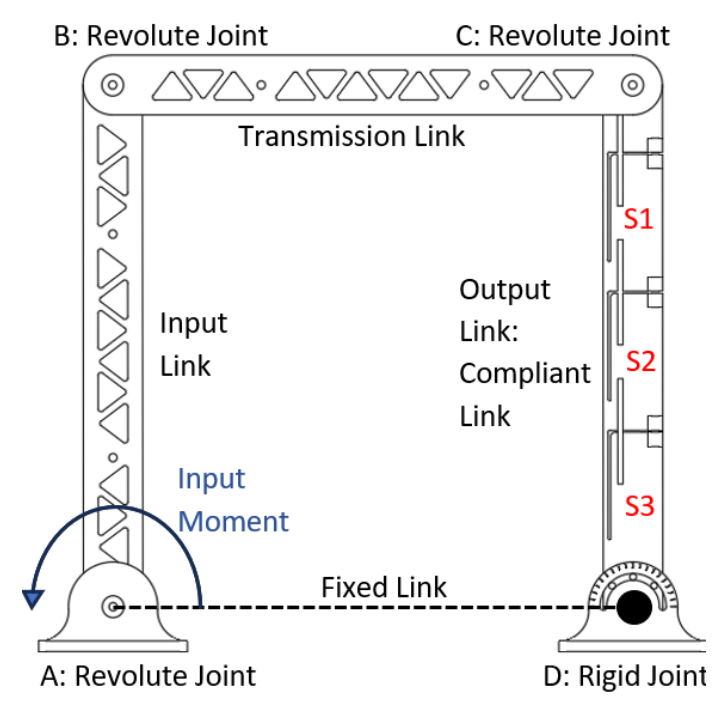


Figure 1: FOUR-BAR MECHANISM WITH SECTIONAL VSL

The design in Figure 1 shows the VSL link as link CD, which is connected rigidly at fixed point D, and to transmission link BC at revolute joint C. The design of VSL allows for a total of eight different configuration sets, each with has unique stiffness profile and deflection behavior. Changing of configuration is achieved by locking two adjacent compliant sections together to form a rigid link, thus changing the effective compliant link length and location of the point of deflection. More details are discussed in section 2.4.

2.1 Variable Stiffness Link Design

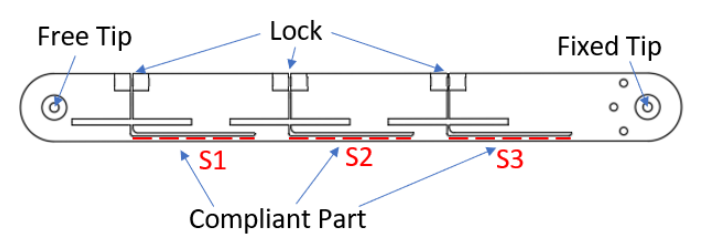


Figure 2: DESIGN OF SECTIONAL VSL

To achieve the goal of adjusting stiffness with all eight configurations, a novel discrete VSL is designed and fabricated. The VSL is unidirectional compliant, allowing only deflection in one direction until the maximum deflection angle is determined by the geometric constraint or the equilibrium constraint determined by the yielding strength of the VSL. The design allows each section to be locked by a pin, either automatically through an actuator, or manually with a passive hatch. The fixed

tip can be rigidly connected to ensure moment load in the VSL body and can be connected with a revolute joint as the VSL becomes fully rigid and serves as a traditional rigid link in the four-bar mechanism.

Figure 3 shows the design of the sectional VSL, where S1, S2, and S3 each can switch between rigid and compliant states by locking the interlink mechanism. According to the design proposed in Figure 3, the configuration sets are categorized into numerical codes with 0 for unlocked compliant parts, and 1 for locked stiff parts in the VSL. The configuration is organized from the free tip end (joint C) to the fixed end (joint D).

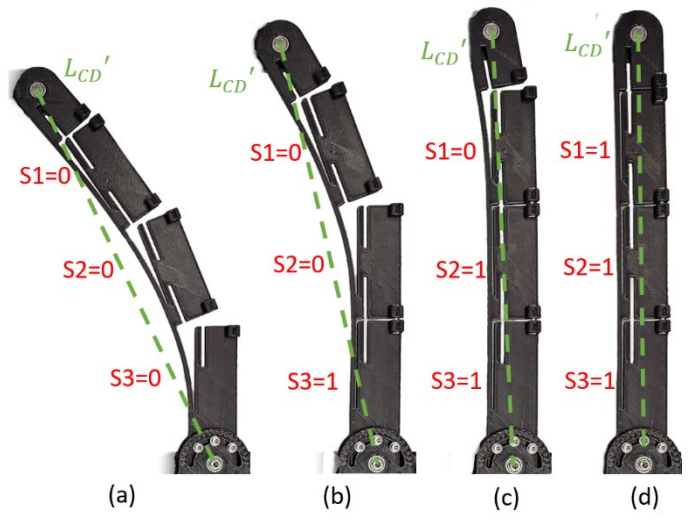


Figure 3: DISPLAY OF VSL CONFIGURATION AT (a) FULLY COMPLIANT, (b) MOSTLY COMPLIANT, (c) MOSTLY RIGID, (d) FULLY RIGID

When a section is unlocked, such a section is considered a compliant part of the whole link. In Figure 3(a), all sections S1, S2, and S3 are in an unlocked state, so the VSL becomes equivalent to a fully compliant link; in Figure 3(b), S3 is locked, and the VSL is now considered to have only 2/3 of the original effective deformable length as S3 is now considered as a rigid part. At such a state, the deflection starting point becomes the ending of S3 from the fixed joint D. From Figure 3, the VSL is shown to have each section independently configured to be rigid or compliant with the locking mechanism, allowing a total of eight different configurations, which will be discussed in section 2.4.

Furthermore, when the VSL is configured to be compliant in different settings, the equipment length of the link CD is changing: $L_{CD}^{\prime(a)} < L_{CD}^{\prime(b)} < L_{CD}^{\prime(c)} < L_{CD}^{\prime(d)} = L_{CD}$. This feature allows the proposed four-bar mechanism with VSL to switch between different trajectories with variation of both configuration and input load.

2.2 Large Deflection Model

The model used to simulate the behavior of the compliant beam is a specific version of PRBM, which follows the mechanical design of the beam structure. The basic calculations for compliant deflection under load are proposed by Su [16]:

$$\sqrt{\alpha} = \frac{1}{2} \int_0^{\theta_{max}} \frac{d\theta}{\sqrt{[\cos(\theta_{max} - \phi) - \cos(\cos(\theta - \phi))] + \kappa}}$$
 (1)

$$a = \frac{l}{2\sqrt{\alpha}} \int_0^{\theta_{max}} \frac{\cos(\theta) d\theta}{\sqrt{[\cos(\theta_{max} - \phi) - \cos(\cos(\theta - \phi))] + \kappa}}$$
 (2)

$$b = \frac{l}{2\sqrt{\alpha}} \int_0^{\theta_{max}} \frac{\sin(\theta) d\theta}{\sqrt{[\cos(\theta_{max} - \phi) - \cos(\cos(\theta - \phi))] + \kappa}}$$
(3)

Which α is the non-dimensional force index, θ is the angle of deflection with respect to the global x-axis, ϕ is the direction of force acting on the free tip of the beam concerning the global x-axis, α and b are the horizontal and vertical deflection of the beam's free tip, l is the length of the beam at straight state, and κ is the load ratio in bending action. The relationships between the force index and load ratio are defined according to Su [16]:

$$\alpha = \frac{Fl^2}{2EI}, \quad \beta = \frac{Ml}{EI}, \quad \kappa = \frac{\beta^2}{4\alpha}$$
 (4)

Where F and M are the force and moment acting on the free tip of the beam, E is Young's module of the material of the beam, and I is the moment of inertia of the beam.

The beam set is used to analyze one complete section of compliant beam starting at horizontal state, so the equations are modified to fit the need of the model. The beam is made as a rectangle shape with 3D printing, and the input for the system is set to be a moment load acting at A. The equivalent force acting on the compliant link CD is calculated to be a force in link BC at joint C. The modified model is shown below:

$$\alpha = \frac{Fl^2}{2EI}, \quad \beta = 0, \quad \kappa = 0, \quad \phi = \pi - \theta_{AD}$$
 (5)

Because the revolute joint at B and C allow only force to be transmitted, moment load at compliant link CD's free tip C is eliminated, resulting in a simplified model where $\kappa=0$. The angle of force will be the same as link BC with respect to the global x-axis, which can be calculated with geometric constraints of the four-bar mechanism. Due to the vertical setup, the deflection of horizontal and vertical also needs to be justified. Therefore, the model can be simplified as:

$$\sqrt{\alpha} = \frac{1}{2} \int_0^{\theta_{max}} \frac{d\theta}{\sqrt{\cos(\theta_{max} - \theta) - \cos(\cos(\theta + \phi))}}$$
 (6)

$$a = \frac{l}{2\sqrt{\alpha}} \int_0^{\theta_{max}} \frac{\cos(\theta) d\theta}{\sqrt{\cos(\theta_{max} - \theta) - \cos(\cos(\theta + \phi))}}$$
 (7)

$$b = \frac{l}{2\sqrt{\alpha}} \int_0^{\theta_{max}} \frac{\sin(\theta) d\theta}{\sqrt{\cos(\theta_{max} - \theta) - \cos(\cos(\theta + \phi))}}$$
(8)

In the experiment, the initial θ is set to be $\pi/2$ as the beam is initially vertically aligned with the y-axis, and $\theta_{AD} = 0$ as both

points A and D are on the x-axis and making $\phi = \pi$ for the force F starts from the negative x-axis direction, as shown in Figure 4.

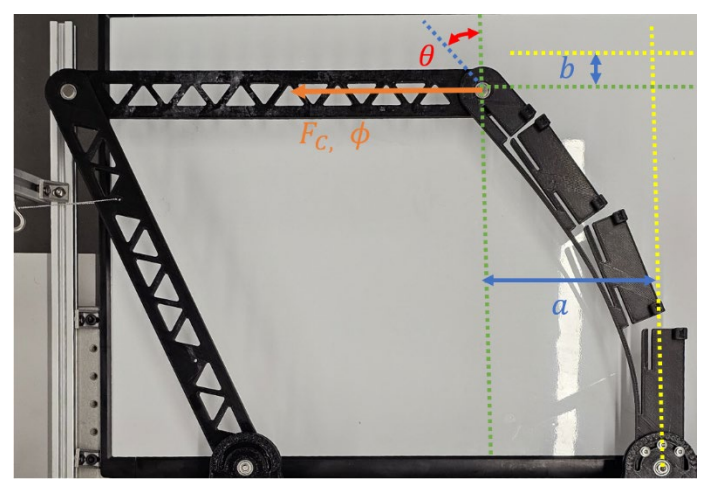


Figure 4: FOUR-BAR MECHANISM WITH VSL SETUP

2.3 Four-bar Loop Closure

Similar to the traditional rigid four-bar mechanism, the system is subject to loop closure constraints. The nature of being a closed loop despite the compliant link CD introduced in this study allows two conditions for the system to be analyzed and solved in the model. The first set is the geometric constraints for each joint of the four-bar mechanism. The geometric constraints for the four-bar mechanism in 2D are expressed as below:

$$|L_{AB}\cos(\theta_{AB})| + |L_{BC}\cos(\theta_{BC})| + |\delta x_{CD}| = L_{AD}$$
 (9)

$$|L_{AB}\sin(\theta_{AB})| + |L_{BC}\sin(\theta_{BC})| + |\delta y_{CD}| = 0$$
 (10)

$$\theta_{max} = \begin{cases} \phi + \cos^{-1}(1 - \kappa), & 0 \le \kappa \le 2\\ \infty, & \kappa \ge 2 \end{cases}$$
 (11)

Equations (9) and (10) are the horizontal and vertical component constraints of the four links, which assume the ground link AD is rigid and fixed in global space. δx_{CD} and δy_{CD} are the horizontal and vertical deflections, which are derived from equations (7) and (8) as α and β . Equation (11) constrains the maximum angle of deflection, which is dependent on the curvature of the compliant link CD. However, as assumed in equation (5), without a tip moment load, the curvature κ at the tip is set to be 0, resulting in:

$$\theta_{max} = \phi = \pi - \theta_{AD} \tag{12}$$

Where the maximum angle of deflection will be equal to the direction of force loading at the compliant beam CD's tip. Geometrically this condition allows link BC and CD to be parallel, resulting in all force acting in the axial direction of link CD's bending tip, causing no more deflection. In the experiment setup, the maximum angle of deflection is π .

The second set of constraints is the static equilibrium constraints. Assume that at any given moment, the internal

moment of the four-bar mechanism is at equilibrium, where the input moment is neutralized by the induced stress in the compliant link CD. Therefore, the sum of moments around point A should be zero when the system is in static equilibrium. The moment M applied at point A induces a reaction force F_C at point C and the resulting moment due to the deflection of link CD must be considered as:

$$M - F_C L_{BC} \sin(\theta_{BC}) - F_C \delta x_{CD} = 0 \tag{13}$$

With both geometric and static equilibrium constraints described in Equ. (9-13), the four-bar mechanism can be solved and kept realistic.

The moment load along the compliant link CD, however, is different everywhere on the link, which is caused by the force load acting only at point C. So, during the elliptical integral approach for the curvature calculation, the moment load should be calculated as:

$$M(i) = F_C(a - y) + nP(b - x)$$
(14)

$$\kappa = \frac{d^2\theta}{ds^2} = -\frac{F_c}{EI}(\sin(\theta) + n\cos(\theta))$$
 (15)

Where x and y are points along the compliant beam CD, s is the complaint link length, n is the nondimensional deflection factor, which is dependent on the force direction as:

$$n = \frac{1}{\tan(\phi)} \tag{16}$$

2.4 Design of Experiment

The experiment is conducted with a 3D-printed four-bar mechanism structure. The compliant link CD mimics a 3PRBM structure by having three lockable compliant sections. With three sections and each section has two states of 0 (unlocked, free to deflect) and 1 (locked, equivalent to rigid link), the system can be configured into a total of eight different configuration sets, similar to the discrete variable stiffness gripper developed by Fu's team [17]. The different configuration allows the maximum moment to be applied at different locations along the compliant beam, which results in different deflection under the same load. A set of experiments was conducted with a simulation of the four-bar mechanism under the same force load.

S1-S2-S3	DESCRIPTION				
0-0-0	Fully compliant				
0-0-1	Mostly compliant top				
0-1-1	Mostly rigid bottom				
1-0-0	Mostly compliant bottom				
1-1-0	Mostly rigid top				
0-1-0	Rigid center				
1-0-1	Compliant center				
1-1-1	Fully rigid				

Table 1: CONFIGURATION SET

The possible configurations shown in Table 1 are used to create corresponding MATLAB simulations according to the two proposed constraints stated in section 2.1-2.2, where all configurations are subjected to the same moment load, which is shown in section 2.41. All links are set to be 350 mm in length to align with the physical prototype, and fixed joint CD is set to be the global origin where the compliant link CD initially aligns with the y-axis in a positive direction. A computational static analysis is done through FEA, which shows the moment and force analysis of the design. The experiment is set up to recreate the predicted behaviors of the simulation as a verification of the modeling, where all eight configurations are achieved.

The experimental VSL is fabricated through the additive manufacturing process of 3D printing. The material used for the VSL is a standard off-the-shelf PLA filament. Fu's team [18] tested and determined the material properties of the PLA used. The test resulted a Young's module E of 3.364GPa and Poisson's ratio according to the negative of the ratio of transverse strain to axial strain to be 0.39 [18].

2.4.1 PRBM Simulation

The simulation is created numerically in MATLAB as all the symbolical constraints and conditions proposed in equations (5)-(8) and (9)-(16) are transformed into numerical solver functions in the same manner as Wu [3] and Chuenchom [14].

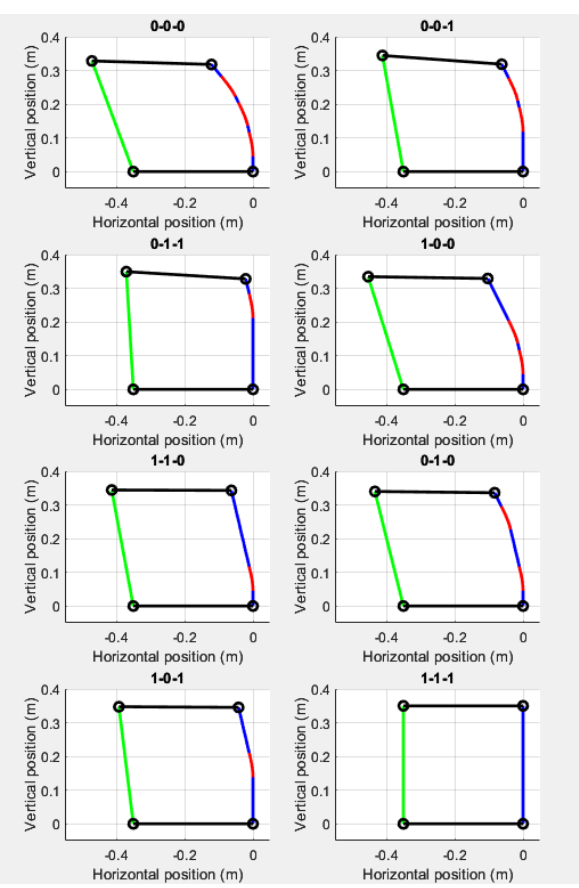


Figure 5: PRBM SIMULATION ON ALL CONFIGURATIONS

The simulation takes physical properties of the four-bar mechanism with VSL and a moment at joint A as input, then outputs the horizontal and vertical deflection, and free tip deflection angle. The results are plotted in Figure 5.

2.4.2 Testing

A set of experiments was conducted to have the same configuration subject to various moment loads. The moment load increases from 0 to maximum load in both the simulation and the physical experiment, Figure 6 shows the comparison. In this section, the maximum compliant configuration 000 is selected and the results of PRBM, FEA, and experiment snapshot are compared to show the differences. A comparison between the experiment and the PRSM simulation is made where six moment loads applied to the VSL during the maximum deflection experiment are inputted into the simulation for model verification.



Figure 66: CONFIGURATION 000 UNDER VARIOUS MOMENT LOAD

The testing includes slightly more error as in the experiment a force load instead of a moment load is used, which though recreated in simulation through computational methods, still varies from reality. The difference is discussed further in section 3 as the error source are discovered.

2.4.3 FEA Simulation

The same moment load is then applied to the design model in ANSYS for each configuration to compare with the numerical simulation and the experiments. The FEA simulation was conducted using a static analysis. The calculated moment was applied to the base of the input link of the VSL. The setup of the

simulation fixed the base of the VSL and added a revolute joint between all rotation joints of the design. The relation between all the links were set as frictionless, allowing the effects of friction in the design to be ignored and the relation between the VSL and the locking pins were set to bonded, depending on the configuration of the simulation.

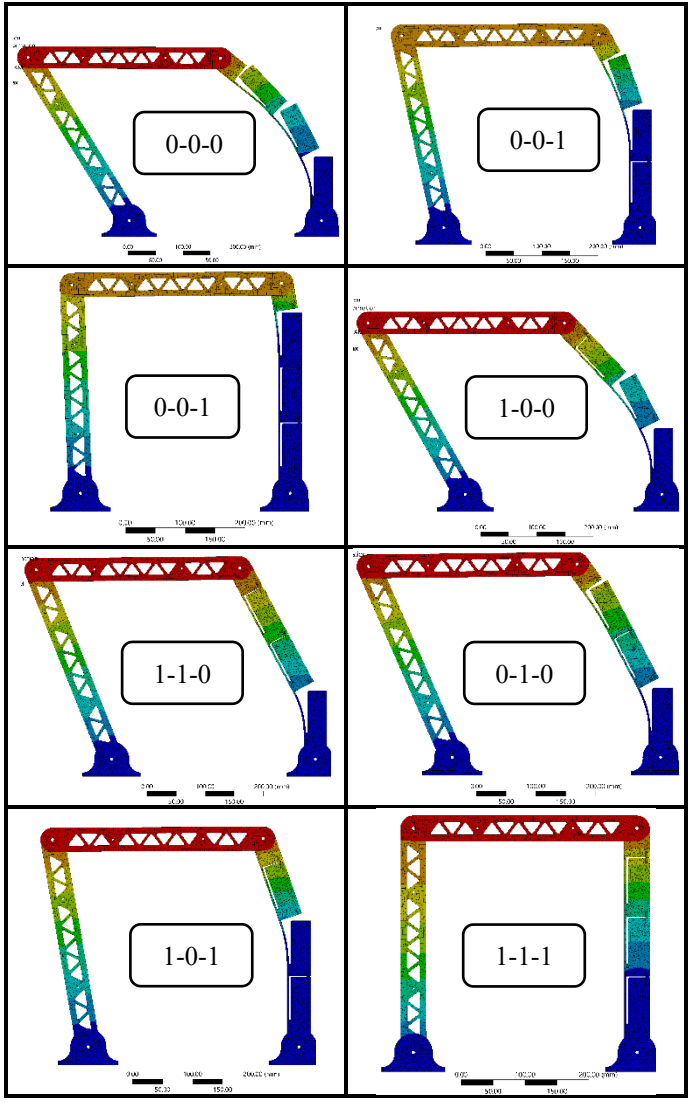


Figure 7: FEA SIMULATION RESULTS FOR ALL CONFIGURATIONS

Furthermore, a non-linear quadratic mesh was selected for the VSL with an average element size of 3.6mm. The density of the mesh was increased further in the bending region of the compliant beam using a face mesh element size of 2.0mm. Finally, the simulation was set to a single step of 1 second with a minimum time step size of 0.01s and large deflections for the simulations were enabled. Each of the configurations were individually setup and tested for deformation based on the input moment to the input link of the VSL as shown in Figure 7.

2.4.4 Physical Experiment

The prototype is fabricated with 3D printed parts and assembled to perform the same input moment and verify the simulation. Due to laboratory setup limitations, the moment load at input link point A is substituted with a force F_A pulling at a point E on the link AB. The direction ψ of force applied to the input link AB is measured and used to calculate the equivalent input moment M at point A, as shown in Figure 8.

$$M = F_A L_{AE} cos (\psi)$$
 (17)

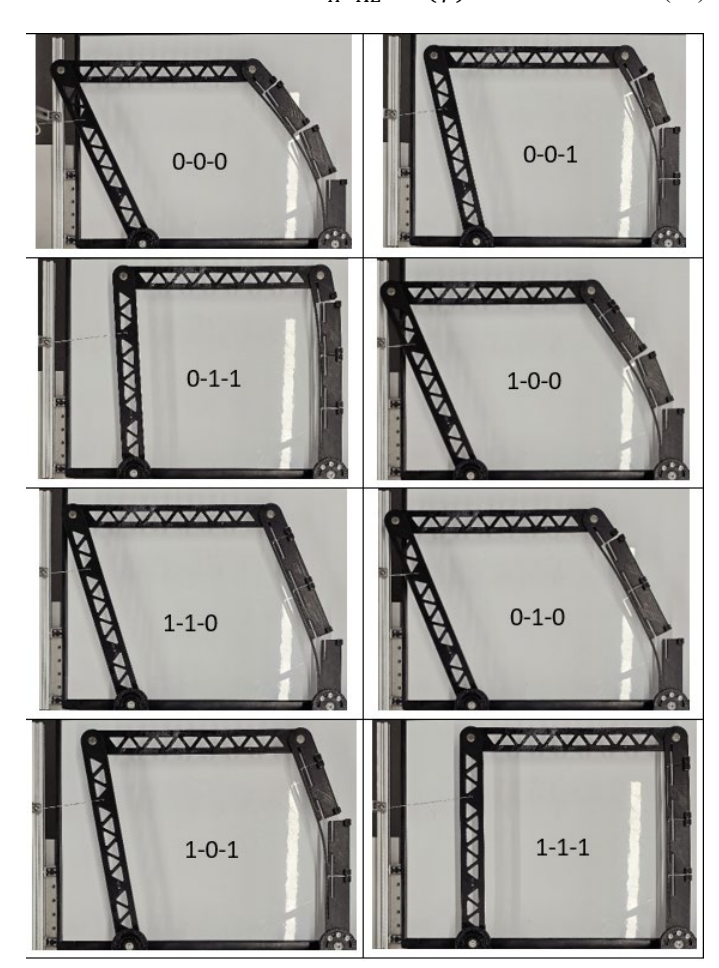


Figure 87: EXPERIMENT ON ALL CONFIGURATIONS

To better reduce the effect of gravity and friction, the experiment is conducted with the four-bar structure horizontally on a smooth surface. Joints A and D are fixed to the surface, ensuring that all surfaces of the four-bar mechanism overlay with the x-y plane. The force F_A is applied by a Mark-10 force gauge, where the direction ψ is measured and the deflection of the free tip of the VSL at joint C is measured by the Mark-10 force gauge. The system is adjusted to generate equivalent torque at joint A for each configuration. Figure 8 shows the experiment results of the conduction, which mostly fit the prediction generated by the PRBM simulation.

The horizontal and vertical displacements are measured at every configuration under the same force load, where the joint C

is used as a reference point using its starting and ending position in the tracking camera.

3. RESULTS AND DISCUSSION

The testing results, FEA results, and simulation results are compared to verify the model's accuracy and ability to predict the deflection of the four-bar mechanism equipped with VSL. From Table 2 it is shown that the error for deflection is generally small and can be seen as acceptable (average error of 11.79%) compared to the FEA results (18.2% average error). The general observation is that when the unlocked part is located closer to the fixed joint C in the VSL, the simulation shows better accuracy with horizontal deflection calculation, especially when section 3 is unlocked. However, when section 3 is locked, the error increases up to 17.08% in configuration 0-1-1. The errors are smaller when the compliant link is configured to have its upper sections (further from the fixed end) locked and lower section unlocked (such as configuration 1-0-0), which essentially is equivalent to a shorter compliant link bending from the same point; and when the compliant link is configured to have its lower section (close to the fixed end) locked and upper section unlocked, the error starts to increase. A hint is given from the fully rigid configuration 1-1-1 where all compliant sections are locked: in the simulation, link CD undergoes no deflection at all, whereas, in reality, the experiment data shows the link still has a small amount of flexibility and can deflect horizontally up to 7 millimeters. FEA shows greater error in deflection verification, which peaks at configuration 0-1-1 at 46%. Again, this configuration caused both FEA and PRBM simulations to have greater errors, proving it is a nonlinear deflection hard to predict.

S1-S2-S3	a _{exp} (mm)	a _{sim} (mm)	a_{FEA} (mm)	err_{sim}	err_{FEA}
0-0-0	121	127.07	130.64	-5.02%	-7.97%
0-0-1	60	65.42	52.54	-9.04%	12.43%
0-1-1	19	22.24	10.20	-17.08%	46.32%
1-0-0	110	108.43	122.93	1.42%	-11.75%
1-1-0	90	86.47	92.15	3.92%	-2.39%
0-1-0	98	87.56	99.81	10.65%	-1.85%
1-0-1	49	44.38	42.31	9.43%	13.65%
1-1-1	7	0.00	0.20	100.00%	97.14%

Table 2: COMPARISON OF HORIZONTAL DEFLECTION

The results for tip deflection angles are compared in Table 3. The PRBM simulation is not very accurate in predicting deflection angle, as the average error is 29.79%. The PRBM calculated is less than the actual deflection angle, which might be caused by the lack of consideration for axial expansion of the VSL under load. FEA simulations show better results, but the error still increases more when upper sections are unlocked and lower sections are locked. Such difference is likely to be caused by a structural error during manufacturing, which caused the link to gain less stiffness.

	θ_{exp}	θ_{sim}	$ heta_{FEA}$		
S1-S2-S3	(deg)	(deg)	(deg)	err_{sim}	err_{FEA}
0-0-0	51.6	41.16	53.46	20.23%	-3.60%
0-0-1	35.4	27.44	30	22.49%	15.25%
0-1-1	16.9	13.72	7.5	18.82%	55.62%
1-0-0	44.6	39.50	45.5	11.43%	-2.02%
1-1-0	31.6	13.72	28.07	56.58%	11.17%
0-1-0	39.2	27.44	38.6	30.00%	1.53%
1-0-1	26.9	13.72	20.3	49.00%	24.54%
1-1-1	8.31	0.00	0	100.00%	100.00%

Table 3: COMPARISON OF TIP DEFLECTION ANGLE FROM VERTICAL

Also due to fabrication limitations, the discrete compliant link has several sections of stiffer sections with wider and thicker structures, which were not accurately reflected in the simulation. Figure 4 shows that most deflection is completed by the "first" compliant section, instead of evenly applied in each section, which is likely to be caused by the force loading at point C, causing uneven moment load along the compliant link CD.

Further investigation of the system setup reveals that the VSL made with PLC material could not fully retain its elasticity after multiple cycles of deflection, resulting in a small offset angle of deflection even in the initial position during the experiment. The measured 0 is 8.31 degrees at configuration 111, which indicates the source of the large error in deflection angle. Also, a unique "snapping" behavior is observed during the experiment, where the VSL would recover its deflection by a small amount once one of the unlocked compliant sections reaches its maximum deflection angle, releasing some stored energy through the backward deformation. This behavior is an expression of the attempt of self-load-balancing, which causes the energy in the VSL to distribute more evenly, but also creates a more nonlinear trajectory in the loading process.

The investigation into the four-bar mechanism equipped with a variable stiffness link (VSL) has underscored its capability to significantly diversify end-effector trajectories. This study's core contribution lies in empirically validating the theoretical model against actual performance metrics, thereby shedding light on the nuanced interplay between VSL configurations and mechanism deflection. The detailed analysis revealed that while the model boasts a commendable degree of accuracy in predicting deflections, notable variances emerge in configurations with different sections of the VSL locked or unlocked. These variances highlight the intricacies of VSL behavior and point toward the necessity for model enhancements and manufacturing precision.

The experimental outcomes, particularly the unanticipated flexibility in configurations presumed rigid, underline the critical role of manufacturing fidelity and the limitations of the current modeling approach in capturing the full spectrum of VSL dynamics. This revelation not only invites a reassessment of the material and structural assumptions inherent in the model but also suggests an avenue for refining the simulation techniques to better mirror real-world behaviors.

The potential application for such a four-bar mechanism has a wide range. The unique advantage of such a design is to have essentially multiple trajectories in one single four-bar mechanism without changing the hardware such as extending the link or shortening the link. The ability to obtain a changeable workspace can be used in various situations, such as automotive windshield wiper, where the four-bar mechanism could reach every corner of the windshield without changing length or moment input, but the stiffness of the cranks. The nature of configurable stiffness also allows the proposed device to serve as a safety damper for shock and vibration absorption, protecting sensitive machinery from sudden impacts.

Moreover, the study illuminates the vast application potential of the proposed four-bar mechanism design, demonstrating its adaptability without the need for physical adjustments. This adaptability is particularly promising for applications requiring dynamic response capabilities, such as automated systems and protective devices against mechanical shocks. In wrapping up, this research marks a significant step forward in the domain of compliant mechanisms, offering a solid foundation for future explorations into VSL-enhanced systems. The findings encourage a deeper dive into optimizing the balance between theoretical models and practical applicability, intending to harness the full potential of variable stiffness in mechanical design. Future work will undoubtedly build on these insights, pushing the boundaries of what is possible in the creation of more responsive, adaptable, and efficient mechanical systems.

4. CONCLUSION

This research highlights the potential of integrating variable stiffness links into four-bar mechanisms to enhance trajectory versatility without structural modifications. Despite the model's generally acceptable accuracy, discrepancies in certain configurations point to the need for further refinement in both simulation and manufacturing processes. The findings pave the way for future advancements in mechanical design, emphasizing the importance of adaptable, efficient systems across a range of applications.

ACKNOWLEDGEMENTS

This work is supported by the National Science Foundation (NSF) grant under CMMI-2131711.

REFERENCES

- [1] J. A. (John A. Hrones, *Analysis of the four-bar linkage; its application to the synthesis of mechanisms*. Cambridge: Published jointly by the Technology Press of the Massachusetts Institute of Technology, and Wiley, New York, 1951.
- [2] R. Karakuş and E. Tanık, "Transmission angle in compliant four-bar mechanism," *International Journal of Mechanics and Materials in Design*, vol. 19, no. 3, 2023, doi: 10.1007/s10999-023-09640-1.
- [3] K. Wu and G. Hao, "Design and nonlinear modeling of a novel planar compliant parallelogram mechanism with general tensural-compresural beams," *Mech Mach*

- *Theory*, vol. 152, p. 103950, 2020, doi: 10.1016/j.mechmachtheory.2020.103950.
- [4] E. Tanik and V. Parlaktaş, "Fully compliant spatial fourbar mechanism," *Journal of Advanced Mechanical Design, Systems and Manufacturing*, vol. 9, no. 1, 2015, doi: 10.1299/jamdsm.2015jamdsm0002.
- [5] M. Ling, J. Cao, Z. Jiang, and J. Lin, "A semi-analytical modeling method for the static and dynamic analysis of complex compliant mechanism," *Precis Eng*, vol. 52, 2018, doi: 10.1016/j.precisioneng.2017.11.008.
- [6] S. Awtar and S. Sen, "A generalized constraint model for two-dimensional beam flexures: Nonlinear loaddisplacement formulation," *Journal of Mechanical Design*, vol. 132, no. 8, 2010, doi: 10.1115/1.4002005.
- [7] J. Fu, H. Lin, I. V. S. Prathyush, X. Huang, L. Zheng, and D. Gan, "A Novel Discrete Variable Stiffness Gripper Based on the Fin Ray Effect," in Lecture Notes in Computer Science (including subseries Lecture Notes in Artificial Intelligence and Lecture Notes in Bioinformatics), 2022. doi: 10.1007/978-3-031-13835-5_71.
- [8] L. L. Howell, *Compliant mechanisms*. New York: Wiley, 2001.
- [9] L. E. Valencia-Segura, M. G. Villarreal-Cervantes, L. G. Corona-Ramirez, F. Cuenca-Jimenez, and R. Castro-Medina, "Optimum Synthesis of Four-Bar Mechanism by Using Relative Angle Method: A Comparative Performance Study," *IEEE Access*, vol. 9, 2021, doi: 10.1109/ACCESS.2021.3115444.
- [10] H. J. Su, H. Shi, and J. Yu, "A symbolic formulation for analytical compliance analysis and synthesis of flexure mechanisms," *Journal of Mechanical Design*, vol. 134, no. 5, 2012, doi: 10.1115/1.4006441.
- [11] H. J. Su, "A pseudorigid-body 3r model for determining the large deflection of cantilever beams subject to tip loads," *J. Mech. Robot*, vol. 1, no. 2, 2009, doi: 10.1115/1.3046148.
- [12] Ashish B. Koli, "A generalized approach for compliant mechanism design using the synthesis with compliance method, with experimental validation," Thesis Open Access, Missouri University of Science and Technology, Rolla, 2013.
- [13] L. L. Howell and A. Midha, "Parametric deflection approximations for end-loaded, large-deflection beams in compliant mechanisms," *Journal of Mechanical Design, Transactions of the ASME*, vol. 117, no. 1, 1995, doi: 10.1115/1.2826101.
- [14] T. Chuenchom and S. Kota, "Synthesis of programmable mechanisms using adjustable dyads," *Journal of Mechanical Design, Transactions of the ASME*, vol. 119, no. 2, 1997, doi: 10.1115/1.2826241.
- [15] J. Fu, H. Lin, I. V. S. Prathyush, X. Huang, L. Zheng, and D. Gan, "A Novel Discrete Variable Stiffness Gripper Based on the Fin Ray Effect," in Lecture Notes in Computer Science (including subseries Lecture Notes in Artificial Intelligence and Lecture Notes in

- *Bioinformatics*), 2022. doi: 10.1007/978-3-031-13835-5_71.
- [16] H. J. Su, "A pseudorigid-body 3r model for determining large deflection of cantilever beams subject to tip loads," *J. Mech. Robot*, vol. 1, no. 2, 2009, doi: 10.1115/1.3046148.
- [17] J. Fu and D. Gan, "A reconfigurable variable-stiffness parallel beam for compliant robotic mechanisms towards safe human interaction," in *Proceedings of the ASME Design Engineering Technical Conference*, 2021. doi: 10.1115/DETC2021-70226.
- [18] J. Fu, Z. Yu, H. Lin, L. Zheng, and D. Gan, "A Novel Variable Stiffness Compliant Robotic Link Based on Discrete Variable Stiffness Units for Safe Human–Robot Interaction," *J Mech Robot*, vol. 16, no. 1, 2024, doi: 10.1115/1.4056957.